Journal of Electroceramics
https://doi.org/10.1007/s10832-021-00250-x

Low temperature sintering of $(Ba_{0.85}Ca_{0.15})$ $(Ti_{0.90}Zr_{0.10})O_3$ lead-free piezoceramic with the additive of MnO_2

Mulualem Abebe Mekonnen[1] · Mesfin Zewdu Tadesse[1]

Received: 23 July 2020 / Accepted: 24 June 2021

Abstract
Lead-free $(Ba_{0.85}Ca_{0.15})$ $(Ti_{0.90}Zr_{0.10})O_3$ (15/10 BCZT) piezoelectric ceramics were prepared by a standard solid solution and sintered at different temperature of 1300 °C and 1500 °C at a time. The 15/10BCZT piezoceramics were prepared at 1300 °C sintering temperature by doping different amount of MnO_2.The ceramics show a phase transition from a freoelectric tetragonal phase to a rhombohedral and tetragonal ferroelctric phase and to a single rhombohedral phase with increasing MnO_2 content. The addition of MnO_2 significantly improves the sinterbility of the 15/10BCZT piezoceramics, and reducing the sintering temperature from 1500 °C to 1300 °C by 200 °C but showing comparable piezoelectric properties. With 0.4 mol% of the dopant, ~96.5% of the theoretical density of the ceramics was achieved with excellent piezoelectric coefficient $d_{33} \sim 534$pC/N, which is nearly equal to the value obtained from the ceramics sintered at 1500 °C which has a piezoelectric coefficient $d_{33} \sim 570$pC/N, high density (~ 5.59 g/cm^3), maximum remnant polarization ($P_r = 24\ \mu C/cm^2$), relatively large grain size (10.4 μm) and the least coercieve field ($E_c = 0.42$ kV/mm). However, a high concentration of MnO_2 deterioated the properties of the ceramics because of increasing of oxygen vacancies and associated defects. The results indicate that the BCTZ-y mol% MnO_2 ceramics are one of the promising lead-free piezoelectric candidates for high temperature applications.

Keywords Piezoelectric coefficient · $(Ba_{0.85}Ca_{0.15})$ $(Ti_{0.90}Zr_{0.10})O_3$ (15/10 BCZT) · Sintering temperature · Lead-free piezoceramics · Microstructure, sintering-aid oxide

1 Introduction

In recent years, $BaTiO_3$-based ceramics have received much attention from the scientific community in the process of searching for the lead-free ferroelectric materials [1–12]. Promising candidates for lead-free piezoelectric ceramics include $BaTiO_3$ (BT), $(K,Na)NbO_3$ (KNN), $(Bi,Na)TiO_3$ (BNT), $(Ba,Ca)(Ti,Zr)O_3$(BCTZ), $(Ba,Ca)(Ti,Sn)O_3$ (BCTS), and $(Ba,Ca)(Ti,Hf)O_3$ (BCHT) [13–16]. Because of their high piezoelectric properties, some researchers Kumar et al. [Kumar Brajesh,1 Khagesh Tanwar,2 Mulualem Abebe,1 and Rajeev Ranjan1 PHYSICAL REVIEW B **92**, 224,112 (2015), Kumar Brajesh, Mulualem Abebe, and Rajeev Ranjan*PHYSICAL REVIEW B **94**, 104,108 (2016)] have reported that BCTZ ceramics can potentially replace lead-based piezoelectric ceramics. Barium titanate-based ceramics is one of the most technologically important ferroelectric oxides with perovskite structure (ABO_3) which is extensively used in electrical industries due to its high dielectric constant [17–20].

Liu and Ren [21] have discovered lead-free $(Ba_{0.85}Ca_{0.15})(Ti_{0.90}Zr_{0.10})O_3$ (15/10 BCZT) ceramics which attractet considerable interest [22–25] due to the excellent piezoelectric properties (with d_{33} = 500–600 pC/N). Some techniques have utilized to improve the piezoresponse value of lead-free piezoelectric ceramics, such as new processing methods, ion substitution, doping of sintering aid oxides and construction of coexistence of two or more phases [26–30]. However, the homogeneous and dense microstructure is quite hard to be obtained in BCZT ceramics, and their sintering temperature are usually required to be as high as 1400 – 1500 °C. These weekness severly limit their practical applications [31–38]. Adding sintering aids is a simple, effective, and commonly used method of lowering the sintering temperature; Wang et al. reported that $(Ba_{0.85}Ca_{0.15})(Ti_{0.9}Zr_{0.1})O_3$ ceramics sintered at 1540 °C have high piezoelectric properties (d_{33} = 650 pC/N) [39]. Li et al. reported that $(Ba_{0.98}Ca_{0.02})(Ti_{0.94}Sn_{0.04})O_3$ and $(Ba_{0.97}Ca_{0.03})(Ti_{0.94}Sn_{0.06})O_3$ ceramics sintered at 1500 °C also

✉ Mulualem Abebe Mekonnen
muabeme@gmail.com

[1] Faculty of Materials Science and Engineering, Jimma Institute of Technology - Jimma University, 1041 Jimma, Ethiopia

Published online: 07 July 2021

have high piezoelectric properties (d_{33} = 510 and 440 pC/N, respectively) [40, 41]. It is thus necessary to use some sintering aids for generating a liquid phase during the sintering process for $BaTiO_3$-based ceramics. Thus, sintering aids can be used to effectively reduce sintering temperature of BCTZ and BCTS ceramics. The effect of MnO_2 as a sintering aid on the sintering temperature, phase structure, microstructure, density, and electrical properties of $(Ba_{0.85}Ca_{0.15})(Ti_{0.90}Zr_{0.10})O_3$ (15/10 BCZT) ceramics were investigated in this study with the aim of lowering the sintering temperature while maintaining high piezoelectric properties.

Zhao et al. reported that $(Ba_{0.95}Ca_{0.05})(Ti_{0.90}Sn_{0.10})O_3$ ceramics reduced its sintering temperature to 1300 °C while retaining high d_{33} values of 485 and 457 pC/N by adding Li_2O_3 or Li_2O as a sintering aid, respectively [42, 43]. Zhou et al. reported that using CuO or LiF as a sintering aid for $(Ba_{0.95}Ca_{0.05})(Ti_{0.90}Sn_{0.10})O_3$ ceramics reduced the sintering temperature to 1250 °C while retaining high d_{33} values of 683 and 510 pC/N, respectively [44, 45]. Chen et al. reported that using ZnO and MnO_2 as sintering aids for $(Ba_{0.91}Ca_{0.09})(Ti_{0.916}Sn_{0.084})O_3$ ceramics reduced the sintering temperature to 1315 °C while mantaining a high d_{33} value of 495 pC/N and found that it increased mechanical quality factor (Qm) due to an increase of oxygen vacancies caused by a small amount of MnO_2 under various sintering temperatures [46]. CuO has been used in $(K_{0.5}Na_{0.5})NbO_3$ (KNN), [39–41] PZT, [42] $Ba_{0.6}Sr_{0.4}TiO_3$, [43] and $(Ba_{1-x}Ca_x)(Ti_{1-y}Zr_y)O_3$ [47–50] ceramics to enhance densification without sacrificing the piezoelectric properties. Hao et al. [51] showed that samples with grain size >10 μm exhibit excellent piezoelectric properties as $d_{33} \sim 470$ pC/N using different sintering methods for BCTZ piezoceramcs.

Uneven grain size distribution makes it difficult to cut ceramics to small dimensions, and polishing thin samples can be problematic. Controlling the sintering regime of seramics is also well known to be critical for the end product's quality [52]. To address these issues, a variety of strategies have been employed. To improve the sinterabiility, a lot of studies have been conducted sinterability by using different sintering aids, for example, a little amount of oxides [53, 54]. Because Mn ions have multivalence states: Mn2+, Mn3+, and Mn4+ [55, 56], MnO2 has been used to simultaneously substitute the A- and B-site cations in order to achieve more stable solid solutions [57–59].

The effect of MnO_2 additive in 15/10BCZT ceramics has not been studied very well. In this study, MnO_2-doped 15/10BCZT ceramics were prepared by an ordinary sintering method and the influence of 0.1 mol% - 1.0 mol% MnO_2 addition on the microstructure, ferroelectric, and piezoelectric properties has been investigated. In addition, Meng et al. [60] reported that the 15/10BCZT ceramic with large grains exhibits high piezoelectricity. Therefore, the possible relationship between electrical properties and grain size were briefly investigated by doping the 15/10BCZT ceramics with different concentration of MnO_2 but sintered at 1300 °C.

2 Experimental

Barium carbonate (BaCO3, 99.8%; Alfa Aesar), calcium carbonate ($CaCO_3$ (99.99%; Alfa Aesar), titanium dioxide (TiO_2, 99.8%; Alfa Aesar) and ZrO_2 were used as raw materials. These powders were weighed according to the composition of $(Ba_{0.85}Ca_{0.15})$ $(Ti_{0.90}Zr_{0.10})O_3$ (15/10 BCZT) was prepared via a conventional solid-state route, then were thoroughly mixed in zirconia jars with zirconia balls and acetone as the mixing medium using a planetary ball mill (Fritsch P5). The slurry was dried and calcined at 1100 °C for 4 h. Thereafter, calcined powders were remixed and pressed into disks of 10 mm in diameter and 1.5 mm in thickness under 98,066.5 N (10 ton) using 2 wt% polyvinyl alcohol as the binder, followed burning the binder at 500 °C by 5 °C/min and for 1 h for all samples. After burning the binder, the samples were cooled to room temperature and then the temperature rose directly from room temperature to sintering temperature of 1300 °C for one set of samples and to sintering temperature of 1500 °C for the other set of samples for 6 hat the rate of 5 °C/min. The specimens were coated with silver paint on the upper and bottom surfaces and fired at 600 °C for 30 min for the electrical measurement.The $(Ba_{0.85}Ca_{0.15})$ $(Ti_{0.90}Zr_{0.10})O_3$ + y mol% MnO_2, (BCTZ + y mol% MnO_2), were prepared by a conventional ceramics technique. The powders in the stoichiometric ratio of the compositions were mixed thoroughly in ethanol using ZrO_2 balls for 12 h, and then dried and calcined at 1100 °C for 4 h in air. After the calcination, the mixture was wet ball-milled again for 6 h dried and granulated with 2 wt% PVA as a binder, and then pressed into green disks with diameters of 12 mm and thickness1.5 mm under a pressure of 10 ton (98,066.5 N). After burning off PVA at 500 °C for 1 h the disk samples were finally sintered at 1300 °C for 6 h in air. The coated samples were poled under a dc field of 2.4 kV/mm at room temperature for 1 h in a silicone oil bath. Room temperature x-ray powder diffraction was done using a Rigaku SmartLab with Johanson monochromator in the incident beam to remove the Cu-Kα_2 radiation. The density ρ was measured by the Archimedes' method. Measurement of the direct weak-field longitudinal piezoelectric coefficient (d_{33}) was carried using piezotest PM 300 by poling the pellets at room temperature for 1 h at a field of ~2.2 kV/mm. Microstructure of the sintered pellets was recorded by Scanning Electron Microscopy (ESEM, Quanta) after gold sputtering the pellets for 6 min. For the SEM image analysis, we used imagej software. For electrical property measurements, silver electrodes were applied on both side of the polished surfaces of pellets and then baked at 150 °C for 4 h to dry out solvents used for electroding. The strain loop and the polarization electric-field hysteresis loop were measured with a Precision Premier II loop tracer.

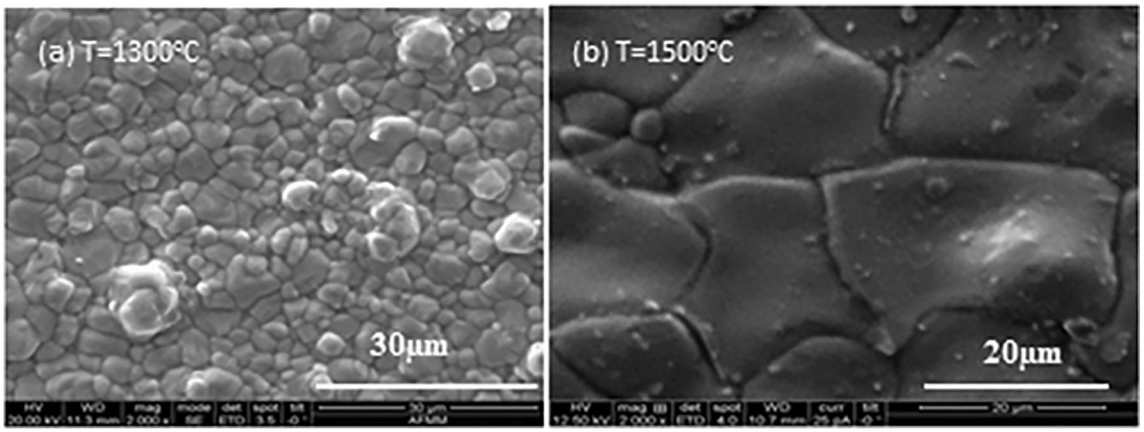

Fig. 1 SEM micrographs of (15/10 BCZT) ceramics sintered at (**a**) 1300 °C and (**b**) 1500 °C

3 Results and discussions

At two different sintering temperatures, lead-free (Ba0.85Ca0.15) (Ti0.90Zr0.10)O3 (15/10 BCZT) piezoelectric ceramics were prepared using the traditional oxide-mixed method. The density and grain size of ceramics, which are closely related to piezoelectric and other properties, are affected by sintering temperatures. The ferroelectric and piezoelectric properties improve as the sintering temperature rises.

Figure 1(a) and (b) show the scanning electron microscope (SEM) images of $(Ba_{0.85}Ca_{0.15})$ $(Ti_{0.90}Zr_{0.10})O_3$ (15/10 BCZT) sintered at 1300 °C and 1500 °C, respectively. In these SEM micrographs, all of the pellets were densely packed grains with typical platy morphology, especially for the sample sintered at 1500 °C. The average grain size determined using the line intercept method revealed that samples sintered at 1300 °C and 1500 °C had grains with average sizes of 4 and 22 µm, respectively, confirming that grain size is strongly influenced by sintering temperature.

Figure 2(a) shows a comparison of the room-temperature x-ray powder differaction profile of BCZT – y mole% MnO_2 ceramics with various MnO_2 sintered at 1300 °C. The data confirmed that all ceramics are consistant with a single phase perovskite and no secondary phases from $2\theta = 15^o$ *to* 90^o. This indicate that the MnO_2 entered the BCZT lattice to form a perovskite structure and solid solution. As shown in Fig. 2(b), the expanded XRD patterns in the 2θ *range of* 44.5^o *to* 46^o. The compositions with y < 0.4 mol% exhibit a tetragonal (P4mm) structure, where the $\{200\}_{pc}$ differaction peak splits in to two with a ratio of 1:2. The compositions with y = 0.4 mol%, 0.6 mol% and 0.8 mol%, the $\{200\}_{pc}$ left side peak started grown up, thus the intensity ratio is not equal to 1:2, unambiguously confirm the presence of other phase in addition to the tetragonal phase which can be justified through

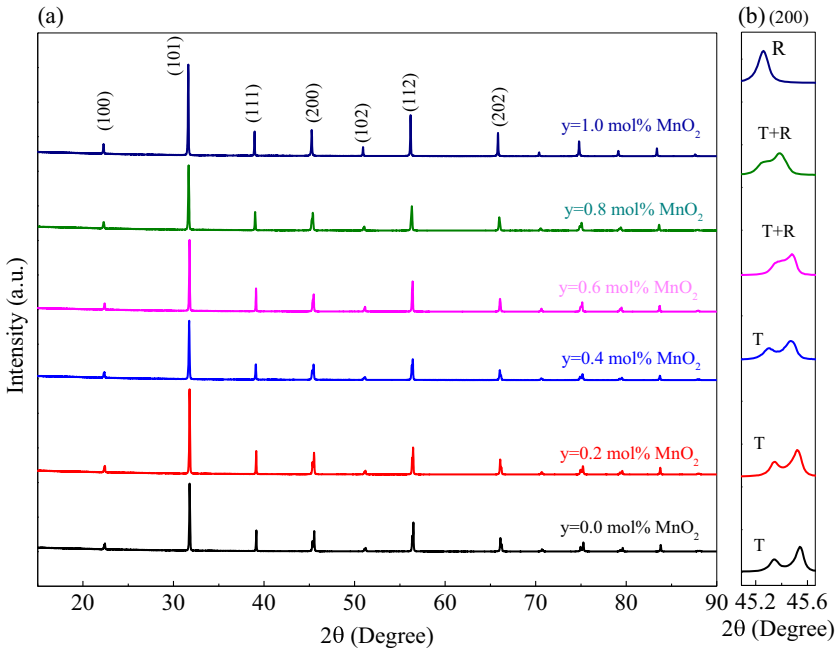

Fig. 2 (**a**) X-ray Bragg profiles of 15/10 BCZT + y mol% MnO_2 and (**b**) the expanded Bragg profile for (200) peak

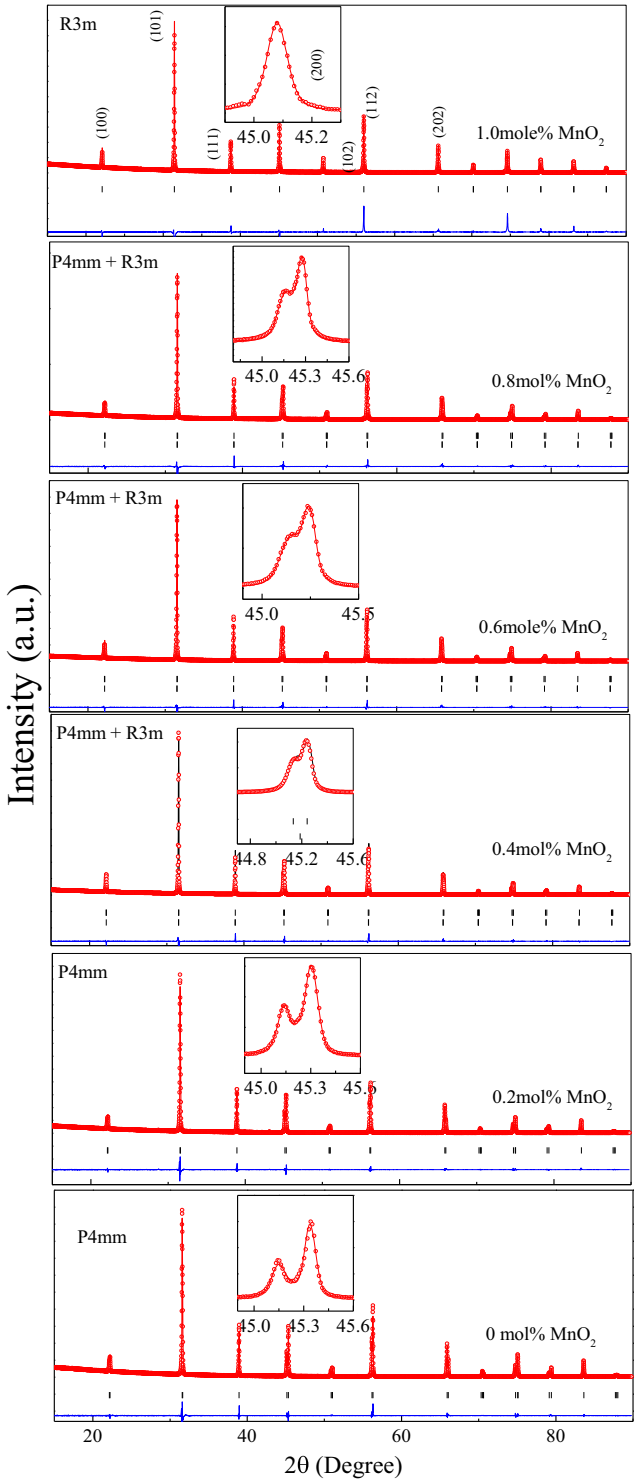

Fig. 3 Rietveld fitted x-ray Bragg profiles of BCZT-y mol% MnO2 sintered at 1300oC using various models (**a**) y = 0 mol% MnO_2, (**b**) y = 0.2 mol% MnO_2, (**c**) y = 0.4 mol% MnO_2, (**d**) y = 0.6 mol% MnO_2, (**e**) y = 0.8 mol% MnO_2, and (**f**) y = 1.0 mol% MnO_2

Rietveld analysis letter on. For y = 1.0 mol%, the $\{200\}_{pc}$ is singlet in conformity with rhombohedral (R3m) structure. As the evolution of the differaction peak of $\{200\}_{pc}$ at y = 0.4 mol% is changed from P4mm phase to R3m + P4mm phase, conforming the involvement of a phase transition. Therefore, the coexistence of tetragonal and rhombohedral phases occurs for the BCZT ceramics with y = 0.4 mol% at room temperature, demonstrating that the ceramics lie at the morphotropic phase boundary (MPB). Rietveld analysis of the x-ray diffraction (XRD) patterns, shown in Fig. 3, confirmed a singlate phase P4mm for y = 0 and 0.2 mol% MnO_2. The compositions with y = 0.4, 0.6 and 0.8 mol% MnO_2 were best fitted with tetragonal (P4mm) + rhombohedral (R3m) phase coexistence models, and the composition with y = 1.0 mol% MnO_2 could be nicely fitted with rhombohedral (R3m) structural model. The refined structural parameters are given in Table 1. Since the peaks move to lower angles, $(Ti, Zr)^{4+}$ is thought to be replaced by Mn^{4+}, implying a change in unit cell volume. This transition may be caused by complete solid solutions forming between the MnO_2 material and the BCZT ceramics, causing crystal lattice distortion. The addition of a solid solution of MnO_2 facilitates the replacement of the Ba^{2+}/Ca^{2+} and/or Zr^{4+}/Ti^{4+} B-sites of the perovskite structure more effectively than raw metal oxides, resulting in increased structure defects and a lower barrier between domains. The formation of the MnO_2 solid solution aids ion diffusion and lowers the sintering temperature of the BCZT.

The microstructure and properties of (15/10)BCTZ after sintering with MnO_2. We decided to keep the sintering temperature constant at 1300 °C and figure out the best sintering help concentration for maximum piezoelectric response. The SEM images of the BCTZ - y mol % MnO_2 ceramics sintered at 1300 °C as a feature of MnO_2 material are shown in Fig. 4. Grain-size was measured in microns using the point-to-point measurement tool. Grains were measured at random across the stub for each sample. For the pure 15/10BCZT ceramic, the grain sizes were not very homogeneous in the range of (3.3–4.7 μm). However, after the addition of 0.4 mol% MnO_2, the ceramic becomes dense and the grains become larger (Fig. 4(d)). When the value of y in percent mol was equal to 0.0, 0.1, 0.2, 0.4, 0.5, 0.6, and 0.8, the average grain size was 4 (±0.71), 6.3 (± 0.56), 9.8 (± 1.55), 10.4 (± 0.56), 7.2 (± 0.70), 6.4 (± 0.69), and 5.2 (± 0.42) μm, respectively. Figure 4(h) depicts the average grain size with the error bars dependence on the addition of MnO_2, (y mol % MnO_2) which shows that the grain size of the ceramics abruptly increased with the increase in y from 0 to 0.4 mol% MnO_2. However, the SEM micrograph in Fig. 4(e, f & g) shows that further increasing the amount of MnO_2 to 0.5, 0.6 and 0.8 mol% gives rise to an abnormal grain boundary, and the average grain size also reduced. It is expected that Mn-ions are homogeneously dissolved in 15/10BCZT ceramics when the MnO_2 addition is ≤0.4 mol%, but further addition of MnO_2 will inhibit grain growth due to accumulation of Mn-ions at the grain boundary. Liquid phase sintering may have been responsible for the increased grain size at 0.4 mol% MnO_2.

Table 1 Properties of BCTZ system as a function of MnO_2 content

MnO_2 content (y in %)	Pr (μC/cm^2)	Strain (%)	d_{33} (pC/N)	Grain size (μm)
0	11.35	0.130	252	4.00
0.2	22.70	0.120	470	9.80
0.4	24.00	0.195	534	10.40
0.6	19.60	0.155	404	6.40
0.8	16.30	0.152	334	5.20

As shown in Fig. 5, it has been observed that the 15/10BCZT – y mol% MnO_2 ceramics without MnO_2 – doping have a low bulk density of 5.42 g cm^{-3} (relative density ~ 95.5%). However, after the doping of 0.2–1.2 mol% MnO_2, all the ceramics give a high density of 5.46–5.59 g cm^{-3} (relative density > 95.7%). The maximum experimental value of 5.59 g/cm^3 (relative density – 96.5%) is obtained for the 0.40 mol% MnO_2-modified BCZT ceramics sintered at 1300 °C. By adding MnO_2 with low melting points, the liquid formation promotes the sintering of BCZT ceramics and results in an increase in the density of the ceramics. However, with increasing the MnO_2 content, the density decreases. This is may be due to a larger amount of this liquid phase accumulating at the grain boundaries, thus resulting in voids and inhibiting densification. It is apparent that adding a small amount of MnO_2 causes the generation of oxygen vacancies is beneficial to the mass transport in the ceramics during sintering, which is responsible for the enhanced grain growth behavior, sinterability and bulk density of the suitable MnO_2-doped specimens sintered at low temperature. When 0.2 mol% of MnO_2 is added, the grains become noticeably larger and more uniform, as can be seen in Fig. 4c. As a result, the ceramic became well sintered and relatively thick, resulting in a substantial increase in densification and grain growth.Therefore, the addition of MnO_2 plays an important role in the improvement of the density of BCZT-based ceramics.

Figure 6(a) illustrates the typical polarization levels versus applied electrical field (P–E) hysteresis loops of MnO2-modified BCZT ceramics sintered at 1300oC and measured with Precision premier II loop tracer at room temperature under an electric field of 35 kV/cm and 1 Hz frequency. Figure 6(a) demonstrates that the P–E hysteresis loops become much slimmer when MnO2 additives are mixed into the BCZT ceramics. Figure 6(b) depicts the remnant polarization (Pr) and coercive field (Ec) of the ceramics as a function of the MnO2 content. According to Fig. 6(b), with increasing the MnO2 content, Pr has minimum value for pure BCZT, then increases and reaches the maximum value of 24 μC/cm^2 when y = 0.4 mol% MnO2 co, indicating that the ceramics with y = 0.4 mol% are the easiest to pole. Moreover, further increasing the MnO2 content beyond 0.4 mol% causes sudden drops in the Pr values, which can be attributed to MnO2 segregation at boundaries which inhibits the movement of domain walls. In addition, it can be observed that Ec of the ceramics markedly decreases from 0.58 kV/mm at y = 0 mol% MnO2 to 0.42 kV/mm at y = 0.4 mol% MnO2 contents. The ceramics with y = 0.40 mol% possess a large Pr (24 μC/cm^2) and a relatively small Ec (0.42 kV/mm). The addition of the MnO2 content affects the polarizability and reduces the Ec values due to the doping effect and the decrement of the lattice parameters. The Rietveld refinement results reveal that the presence of Mn ions induced slight variations in the cell parameters (a decrease in the cell parameter) and a slight increase in the tetragonality (the value of c/a from 1. 00026 to 1.0030) as indicated in Table 2. Considering that the ionic radii of both Zr^{4+} (r = 0.72 Å) and Ti^{4+} (r = 0.605 Å) are larger than that of Mn^{4+} (r = 0.53 Å) or Mn^{3+} (r = 0.58 Å), it is reasonable to sepeculate that some Mn^{4+} or Mn^{3+} ions enter B-site of BCZT crystalline lattice in MnO_2-modified BCZT ceramics which leads to a lattice distortion and an accompanying slight decrease in the lattice parameters, shown in Fig. 7. A lower Ec value is

Table 2 The Rietveld refinement results for the MnO_2-doped BCZT ceramics

Content of MnO_2 (mol%)	0.00	0.20	0.40	0.60	0.80	1.00
a_T(Å)	4.00337	4.00218	4.00186	4.00041	4.0003	–
c_T(Å)	4.00441	4.00327	4.00305	4.00286	4.00152	–
c_T/a_T	1.00026	1.00027	1.00029	1.00061	1.00030	
a_R (Å)			5.67358	5.66997	5.66755	5.66829
c_R(Å)			6.9754	6.94953	6.94143	6.97027
The goodness of fit parameter (χ^2)	1.31	1.68	2.13	1.83	1.99	2.16

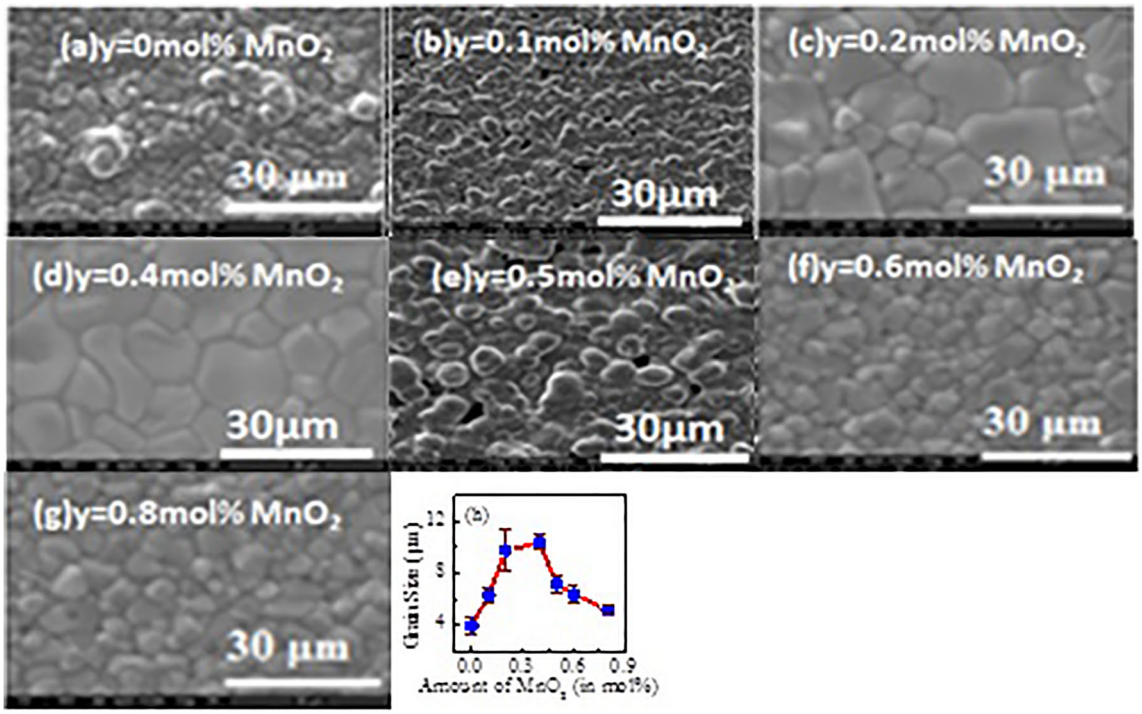

Fig. 4 SEM micrographs of 15/10BCTZ – y mol% MnO2 ceramics sintered at 1300 °C with (**a**) y = 0.0, (**b**) y = 0.1, (**c**) y = 0.2, (**d**) y = 0.4, (**e**) y = 0.5, (**f**) y = 0.6 (**g**) y = 0.8

advantageous in the fabrication of high-density and low-operation-voltage sensors and actuators [61]. The ceramic with y = 0.8 mol% exhibits a relatively large Ec (0.53 kV/mm) and a small Pr (16.35 μC/cm^2), because MnO2 doping is expected to increase the defect concentration either at the A- or B-site of the ABO3 lattice, a direct interaction of these defects with the domain walls is expect [62, 63].

As observed in Fig. 6(b), the piezoelectric constant (d_{33}), and remnant polarization (P_r) change with the MnO_2 content increases, reaching the maximum values at the same time, and then droping simultaneously but the E_c showed the opposite trend. The surprising increase of d_{33} and P_r and the decreasing of E_c – values at y = 0.4 mol% MnO_2 are related to their ferroelectric properties. Moreover, the dense microstructure is also partly responsible for the enhanced piezoelectric properties observed in this work [64].

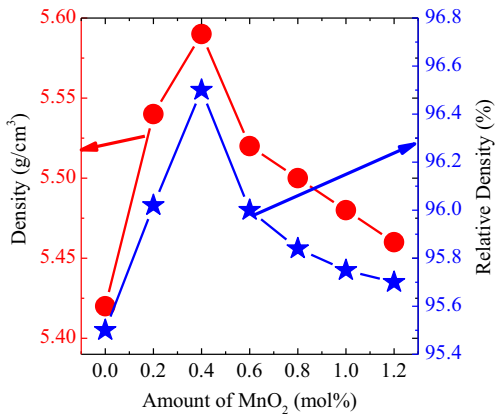

Fig. 5 The relative density and density of the BCTZ - y mol%MnO_2 ceramics sintered at 1300 °C as a function of amount of MnO_2 content

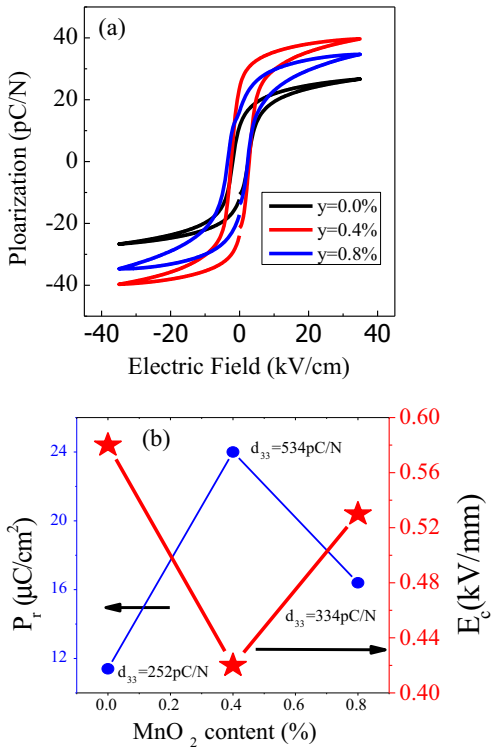

Fig. 6 (**a**) P-E loops, (**b**) P_r and E_c values as a function of MnO_2 content of the BCZT ceramics sintered at 1300 °C and measured at room temperature under an electric field of 35 kV/cm and 1 Hz frequency

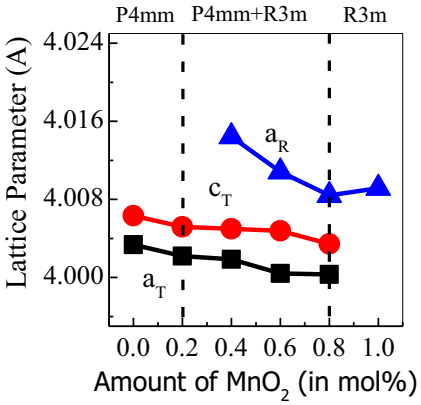

Fig. 7 Lattice parameters as a function of MnO_2 (in mol%) content. The subscripts T, and R correspond to tetragonal and rhombohedral, respectively

It can be seen in Fig. 8, the piezoelectric response (d_{33}) and grain size all change with MnO_2 content, reaching a maximum value when y = 0.4 mol% and then decreasing as we move away from y = 0.4 mol%. On the basis of the Avrami model, Orihara suggested the theory of grain size dependent P-E hysteresis loop [65]. The enhancement of the remnant polarization is due to the increase in grain size as per the relation of $f = [1 - \exp(-G_a d^3/kT)]$, where f is the proportion of grains contribution in polarization reverse, G_a is the grain anisotropy energy density, d is the grain size. Based on the above relation, the number of grains contributing in polarization reverses increases with the increasing grain size, giving rise to the enhancement of the remnant polarization P_r.

Figure 9 illustrates the bipolar electric-field-induced strain of the BCZT ceramics as a function of MnO_2 contents. As observed in Fig. 9(a), the ceramics all exhibit the typical butterfly-shaped curve of ferroelectrics and the electric-field-induced strain of the 15/10 BCTZ ceramics also shows a strong dependence on the grain size. From Fig. 9(a), the bipolar maximum strain of the ceramics is 0.195%, which is obtained at y = 0.4 mol%, and then significantly decreases from 0.195% to 0.152% with the increasing of the content of

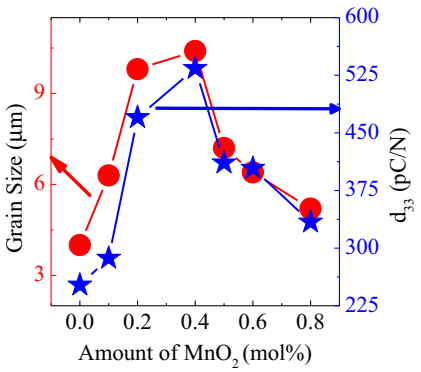

Fig. 8 Piezoelectric response (d_{33}) and average grain size as a function of MnO_2 content of the BCZT ceramics sintered at 1300 °C and measured at room temperature

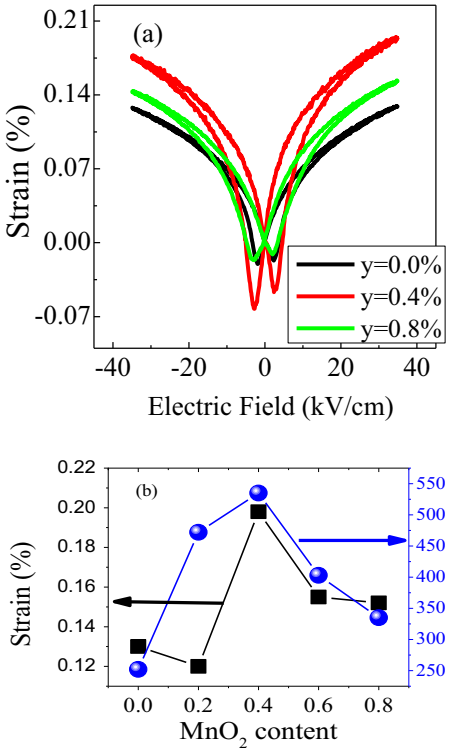

Fig. 9 The strain and piezoelectric properties of BCZT ceramics as a function of MnO_2 content sintered at 1300 °C measured at room temperature under an electric field of 35 kV/cm and 1 Hz frequency

MnO_2. Generally speaking, a large electric-field-induced strain means a large piezoelectric response. The results for the electric-field-induced strain are consistent with the d_{33} values, the size of grain and the increament of remenant polarization as per the relation $d_{33} = 2Q_{11}.P_r.\varepsilon_{33}$,[39] where d_{33} is the piezoelectric coefficient, Q_{11} is the electro-strictive coefficient, ε_{33} is the dielectric constant. Jigong et al.[66] has reported that all the piezoelectric parameters piezoelectric constant d_{33}, electromechanical coupling factor k_p, and S_{max}/E_{max} (the dynamical piezoelectric coefficient d^*_{33}) show reduced value with grain size reduction.

Since the structural activities of the compositions in the biphase coexisting regions are strong, the phase transition from the rhombohedral ferroelectric phase to the tetragonal phase, as well as ion mobility and polarization, may happen quickly. This structural transition is very beneficial in enhancing the strain properties. It can also be seen in Fig. 9(b) that d_{33} decreases from 534 pC/N to 334 pC/N for the ceramics with increasing the content of MnO_2 from 0.4 wt% to 0.8 wt%. The lattice distortion and domain switching induced by electric field contribute to the measured strain. Meanwhile, only lattice distortion contributes to the d_{33} value measured by the quasistatic method. E_c of the ceramics in Figs. 6(b) shows minimum value with the MnO_2 content y = 0.4 mol%, and the ceramics grain size exhibiting the maximum value (fig. 8) at the same time; therefore, the domain switches more easily.

The joint action of lattice distortion and domain switching results in the largest strain being obtained in the 0.40 mol% doped - BCZT ceramics. Properties of BCZT with content of MnO_2 are given in Table 2.

4 Conclusions

BCZT lead-free piezoelectric ceramics with various MnO_2 contents were prepared using the conventional solid state sintering method. The phase structure, microstructure, and ferroelectric properties of the BCZT ceramics as a function of the MnO_2 content were investigated in this study. The results demonstrated that the addition of MnO_2 content not only decreased the sintering temperature but also retained the optimum electrical properties. The sintering temperature of BCZT can be decreased from 1500 °C to 1300 °C with the addition of 0.4 mol%-MnO_2; therefor, the sintering temperature has reduced by 200 °C than that for pure (15/10) BCTZ ceramics while showing comparable piezoceramic properties. The coexistence of tetragonal and rhombohedral phases (MPB) was identified for the BCZTceramics at y = 0.4 mol%, as confirmed by the XRD patterns. Due to the existence of MPB around y = 0.4%, the optimum electrical properties of d_{33} = 535 pC/N, and Pr = 24 $\mu C/cm2$ were obtained in 0.4 mol% MnO_2 doped BCZT ceramics. The introduction of the diffusion mechanism into BCZT ceramics improved the temperature stability of the piezoelectric properties, which was useful in other material systems. MnO_2 additives also gave the piezoceramics the largest grain size, the highest piezoelectric constant, the best density, and the smallest coercive area. These findings suggested that adding MnO_2 to BCZT ceramics would boost their electrical properties significantly. The current research found that $((Ba_{0.85}Ca_{0.15})(Ti_{0.90}Zr_{0.10})O_3$–0.4 mol% $MnO_2)$ ceramics with a low MnO_2 content.

Acknowledgments Mulualem Abebe acknowledges the Department of Materials Science and Engineering, Indian Institute of Science for financial assistance to the research. Mesfin Zewdu and Mulualem Abebe gratefully acknowledges the Department of Materials Science and Engineering, Jimma Institute of Technology for publication.

Data availability The datasets supporting the conclusions of this article are included within the article.

References

1. W. Li, J.X. Zhi, Q.C. Rui, F. Peng, Z.Z. Guo, Enhanced ferroelectric properties in (Ba1-xCax)(Ti0.94Sn0.06)O3 lead-free ceramics. J. Eur. Ceram. Soc. **32**, 517–520 (2012)
2. W.F. Liu, X.B. Ren, Large piezoelectric effect in Pb-freeceramics. Phys. Rev. Lett. **103**(25), 257602 (2009)
3. J.G. Wu, D.Q. Xiao, W.J. Wu, J.G. Zhu, J. Wang, Effectofdwelltime during sintering on piezoelectric properties of (Ba0.85Ca0.15)(Ti0.90Zr0.10)O3 lead-free ceramics. J. Alloys Compd. **509**, L359–L361 (2011)
4. M. Tanmoy, R. Guo, A.S. Bhalla, Structure–property phase diagram of BaZrxTi1-xO3 system. J.Am.Ceram.Soc. **91**, 1769–1780 (2008)
5. F. Mouraa, A.Z. Simoes, B.D. Stojanovic, M.A. Zaghete, E. Longoa, J.A. Varela, Dielectric and ferroelectric characteristics of barium zirconate titanate ceramics prepared from mixed oxide method. J.Alloys Compd. **462**(1-2), 129–134 (2008)
6. W. Li, Z.J. Xu, R.Q. Chu, P. Fu, G.Z. Zang, Dielectric and piezoelectric properties of Ba(ZrxTi1-x)O3 lead-free ceramics. Braz. J.Phys. **40**(3), 353–356 (2010)
7. N. Nanakorn, P. Jalupoom, N. Vaneesorn, A.Thanaboonsom but, Dielec-tric and ferroelectric properties of Ba(ZrxTi1-x)O3 ceramics. Ceram.Int. **34**, 779–782 (2008)
8. S.J. Kuang, X.G. Tang, L.Y. Li, Y.P. Jiang, Q.X. Liu, Influence of Zr dopant on the dielectric properties and Curie temperatures of Ba (ZrxTi1-x)O3 (0 < x < 0.12) ceramics. Scr.Mater. **61**, 68–71 (2009)
9. W.Q. Cao, J.W. Xiong, J.P. Sun, Dielectric behavior of Nb-doped Ba(ZrxTi1-x)O3. Mater.Chem.Phys. **106**(2-3), 338–342 (2007)
10. X.G. Tang, J. Wang, X.X. Wang, H.L.W. Chan, Effects of grain size on the dielectric properties and tunabilities of sol–gel derived Ba(Zr0.2Ti0.8)O3 ceramics. Solid State Commun. **131**, 163–168 (2004)
11. Y.L. Wang, L.T. Li, J.Q. Qi, Z.L. Gui, Ferroelectric characteristics of ytterbium-doped barium zirconium titanate ceramics. Ceram.Int. **28**(6), 657–661 (2002)
12. P. Zheng, J.L. Zhang, H.B. Qin, K.X. Song, J. Wu, Z.H. Ying, L. Zheng, J.X. Deng, MnO2-modified Ba(Ti,Zr)O3 ceramics with high Qm and good thermal stability. J.Electron.Mater. **42**(6), 1154–1157 (2013)
13. B. Jaffe, W.R. Cook, H. Jaffe, *Piezoelectric Ceramics* (Academic Press, London and New York, 1971)
14. Y. Saito, H. Takao, T. Tani, T. Nonoyama, K. Takatori, T. Homma, T. Nagaya, M. Nakamura, Nature **432**(7013), 84–87 (2004)
15. J. Rödel, W. Jo, K. Seifert, E.M. Anton, T. Granzow, D. Damjanovic, J. Am. Ceram. Soc. **92**, 1153 (2009)
16. H. Du, Z. Li, F. Tang, S. Qu, Z. Pei, W. Zhou, Mater. Sci. Eng. **B 131**, 83 (2006)
17. A.K. Menon, B.K. Gupta, Nanotechnology: A data storage perspective. Nanostruct. Mater. **11**(8), 965–986 (1999)
18. B.K. Lee, Y.I. Jung, S.-J.L. Kang, J. Nowotny, {111} Twin formation and abnormal grain growth in barium strontium titanate. J. Am. Ceram. Soc. **86**(1), 155–160 (2003)
19. G.H. Haertling, Ferroelectric ceramics: History and technology. J. Am. Ceram. Soc. **82**(4), 797–818 (1999)
20. R. López-juárez, F. González, M.-E. Villafuerte-Castrejón, in *Ferroelectrics – Material Aspects*, ed. by M. Lallart. Lead-free ferroelectric ceramics with perovskite structure (In Tech, Rijeka, 2011), pp. 305–330
21. W.F. Liu, X.B. Ren, Large piezoelectric effect in Pb-free ceramics. Phys. Rev. Lett. **103**(25), 257602 (2009)
22. W. Li, Z. Xu, R. Chu, P. Fu, G. Zang, Piezoelectric and dielectric properties of (Ba1−xCax)(Ti0.95Zr0.05)O3 lead-free ceramics. J. Am. Ceram. Soc. **93**(10), 2942–2944 (2010)
23. M. Porta, T. Lookman, A. Saxena, Effects of criticality and disorder on piezoelectric properties of ferroelectrics. J. Phys. Condens. Matter **22**(34), 345902 (2010)
24. W. Li, Z. Xu, R. Chu, P. Fu, G. Zang, High piezoelectric d33 coefficient in (Ba1-xCax)(Ti0.98Zr0.02)O3 lead-free ceramics with relative high curie temperature. Mater. Lett. **64**(21), 2325–2327 (2010)

25. W. Li, Z. Xu, R. Chu, P. Fu, G. Zang, Polymorphic phase transition and piezoelectric properties of (Ba1-xCax)(Ti0.9Zr0.1)O3 lead-free ceramics. Phys. B Condens. Matter **405**(21), 4513–4516 (2010)
26. J.G. Wu, D.Q. Xiao, W.J. Wu, Q. Chen, J.G. Zhu, Z.C. Yang, J. Wang, J. Eur. Ceram. Soc. **32**(4), 891–898 (2012)
27. M.C. Ehmke, F.H. Schader, K.G. Webber, J. Rodel, J.E. Blendell, K.J. Bowman, Acta Mater. **78**, 37–45 (2014)
28. C.Y. Chang, H.I. Ho, T.Y. Hsieh, C.Y. Huang, Y.C. Wu, Ceram. Int. **39**(7), 8245–8251 (2013)
29. J.G. Wu, A. Habibul, X.J. Cheng, X.P. Wang, B.Y. Zhang, Mater. Res. Bull. **48**(10), 4411–4414 (2013)
30. J.P. Praveen, K. Kumar, A.R. James, T. Karthik, S. Asthana, D. Das, Curr. Appl. Phys. **14**(3), 396–402 (2014)
31. M. Tanmoy, R. Guo, A.S. Bhalla, Structure–property phasediagramof BaZrxTi1_xO3 system. J.Am.Ceram.Soc. **91**, 1769–1780 (2008)
32. F. Mouraa, A.Z. Simoes, B.D. Stojanovic, M.A. Zaghete, E. Longoa, J.A. Varela, Dielectric and ferroelectric characteristics of bariumzirco-nate titanate ceramics prepared from mixed oxide method. J.Alloys Compd. **462**(1-2), 129–134 (2008)
33. W. Li, Z.J. Xu, R.Q. Chu, P. Fu, G.Z. Zang, Dielectric and piezo-electric properties of Ba(ZrxTi1_x)O3 lead-freeceramics. Braz.J.Phys. **40**, 353–356 (2010)
34. N. Nanakorn, P. Jalupoom, N. Vaneesorn, A.Thanaboonsom but, Dielectric and ferroelectric properties of Ba(ZrxTi1_x)O3 ceramics. Ceram.Int. **34**, 779–782 (2008)
35. S.J. Kuang, X.G. Tang, L.Y. Li, Y.P. Jiang, Q.X. Liu, Influence of Zr dopant on the dielectric properties and Curie temperatures of Ba (ZrxTi1-x)O3 ($0 \le x \le 0.12$) ceramics. Scr.Mater. **61**, 68–71 (2009)
36. X.J. Chou, J.W. Zhai, X. Yao, Relaxor behavior and dielectric properties of MgTiO3-doped BaZr0.35Ti0.65O3 composite ceramics for tunable applications. J.Am.Ceram.Soc. **90**, 2799–2801 (2007)
37. C. Ciomaga, M. Viviani, M.T. Buscaglia, V. Buscaglia, L. Mitoseriu, A. Stancu, P. Nanni, Preparation and characterization of the Ba(Zr,Ti)O3 ceramics with relaxor properties. J.Eur.Ceram.Soc. **27**(13-15), 4061–4064 (2007)
38. T. Maiti, E. Alberta, R. Guo, A.S. Bhalla, ThePolarClusterlike Behavior inTi4þ Substituted BaZrO3Ceramics. Matter.Lett. **60**, 3861–3865 (2006)
39. P. Wang, Y. Li, Y. Lu, J. Eur. Ceram. Soc. **31**(11), 2005–2012 (2011)
40. W. Li, Z. Xu, R. Chu, P. Fu, G. Zang, J. Am. Ceram. Soc. **94**(12), 4131–4133 (2011)
41. W. Li, Z. Xu, R. Chu, P. Fu, G. Zang, J. Eur. Ceram. Soc. **32**(3), 517–520 (2012)
42. L. Zhao, B.-P. Zhang, P.-F. Zhou, L.-F. Zhu, J.-F. Li, J. Eur. Ceram. Soc. **35**(2), 533–540 (2015)
43. L. Zhao, B.-P. Zhang, P.-F. Zhou, X.-K. Zhao, L.-F. Zhu, J. Am. Ceram. Soc. **97**(7), 2164–2169 (2014)
44. P.-F. Zhou, B.-P. Zhang, L. Zhao, X.-K. Zhao, L.-F. Zhu, L.-Q. Cheng, Appl. Phys. Lett. **103**(17), 172904 (2013)
45. P.-F. Zhou, B.-P. Zhang, L. Zhao, L.-F. Zhu, Ceram. Int. **41**(3), 4035–4041 (2015)
46. Q. Chen, T. Wang, J. Wu, X. Cheng, X. Wang, B. Zhang, J. Electroceram. **32**(2-3), 175–179 (2014)
47. Y.R. Cui, X.Y. Liu, M.H. Jiang, Y.B. Hu, Q.S. Su, H. Wang, J. Mater. Sci. Mater. Electron. **23**, 1342 (2012)
48. W. Lin, L.L. Fan, D.M. Lin, Q.J. Zheng, X.M. Fan, H.L. Sun, Curr. Appl. Phys. **13**, 469 (2013)
49. P. Zheng, J.L. Zhang, S.F. Shao, Y.Q. Tan, C.L. Wang, Appl. Phys. Lett. **94**(3), 032902 (2009)
50. T. Chen, T. Zhang, G.C. Wang, J.F. Zhou, J.W. Zhang, Y.H. Liu, J. Mater. Sci. **47**(11), 4612–4619 (2012)
51. J. Hao, W. Bai, W. Li, H.T.M. JiweiZhai, J.C. Burfoot, Grain-Size Effects on Properties of Some Ferroelectric Ceramics. J. Phys. C: Solid State Phys. **7**, 3182–3192 (1974)
52. H. Du, Z. Li, F. Tang, S. Qu, Z. Pei, W. Zhou, Preparation and Piezoelectric Properties of (K0.5Na0.5)NbO3 Lead-free Piezoelectric Ceramics with Pressure-less. Sinter. Mater. Sci. Eng. **B 131**, 83–87 (2006)
53. E. Li, H. Kakemoto, S. Wada, T. Tsurumi, Influence of CuO on the Structure and Piezoelectric Properties of Alkaline Niobate-Based Lead-Free Ceramics. J. Am. Ceramic Soc. **90**(6), 1787–1791 (2007)
54. B. Malic, J. Bernard, J. Holc, D. Jenko, M. Kosec, Alkaline-Earth Doping in (K,Na)NbO3 Based Piezoceramics. J. Eur. Ceramic Soc. **25**, 2707–2711 (2005)
55. S.H. Park, C.W. Ahn, S. Nahm, J.S. Song, Microstructure and Pyroelectric Properties of ZnO-Added (Na0.5K0.5)NbO3 Ceramics Japanese. J. Appl. Phys. **43**(8B), 1072–1074 (2004)
56. Y. Hou, M. Zhu, F. Gao, H. Wang, B. Wang, H. Yan, C. Tian, J. Am. Ceram. Soc. **87**(5), 847–850 (2004)
57. M. Dambekalne, M. Antonova, M. Livinsh, A. Kalvane, A. Mishnov, I. Smeltere, R. Krutohvostov, K. Bormanis, A. Sternberg, Synthesis and Characterization of Sbsubstituted (K0.5Na0.5)NbO3 Piezoelectric Ceramics. Integrated Ferroelect. **102**, 52–61 (2008)
58. S. Zhang, R. Xia, T.R. Shrout, G. Zang, J. Wanag, Characterization of Lead-free (K0.5Na0.5)NbO3 – LiSbO3 Piezoceramic. Solid State Commun. **141**, 675–679 (2007)
59. F. Rubio-Marcos, P. Ochoa, J.F. Fernandez, Sintering and Properties of Lead-free (K,Na,Li)(Nb,Ta,Sb)O3. J. Eur. Ceramic Soc. **27**, 4125–4129 (2007)
60. M. Jiang, Q. Lin, D. Lin, Q. Zheng, X. Fan, X. Wu, H. Sun, Y. Wan, L. Wu, J Mater Sci **48**, 1035–1041 (2013)
61. S. Zhang, R.E. Eitel, C.A. Randall, T.R. Shrout, E.F. Alberta, Appl. Phys. Lett. **86**(26), 262904 (2005)
62. R.S. Nasar, M. Cerqueira, E. Longo, J.A. Varela, A. Beltran, J. Eur. Ceram. Soc. **22**(2), 209–218 (2002)
63. R. Eitel, C.A. Randall, Phys. Rev. B **75**(9), 094106 (2007)
64. K. Kinoshita, A. Yamaji, Grain-size effects on dielectric properties in barium titanate-ceramics. J.Appl.Phys. **47**, 371 (1976)
65. H. Orihara, S. Hashimoto, Y. Ishibashi, A theory of D-E hysteresis loop based on the Avrami model. J. Phys. Soc. Jpn. **63**(3), 1031–1035 (1994)
57. J. Hao, W. Bai, W. Li, J. Zhai, J. Am. Ceram. Soc. **95**(6), 1998–2006 (2012)